RESEARCH ARTICLE

Linkage analysis reveals allosteric coupling in Kir2.1 channels

Daniel M. Sigg[1] , Hsueh-Kai Chang[2], and Ru-Chi Shieh[2]

Potassium-selective inward rectifier (Kir) channels are a class of membrane proteins necessary for maintaining stable resting membrane potentials, controlling excitability, and shaping the final repolarization of action potentials in excitable cells. In addition to the strong inward rectification of the ionic current caused by intracellular blockers, Kir2.1 channels possess "weak" inward rectification observed in inside-out patches after prolonged washout of intracellular blockers. The mechanisms underlying strong inward rectification have been attributed to voltage-dependent block by intracellular Mg^{2+} and polyamines; however, the mechanism responsible for weak rectification remains elusive. Hypotheses include weak voltage-dependent block and intrinsic voltage-dependent gating. Here, we performed a conductance Hill analysis of currents recorded with a double-ramp protocol to evaluate different mechanisms proposed for weak inward rectification of Kir2.1 channels. Linkage analysis in the form of a Hill plot revealed that the ramp currents could be best explained by allosteric coupling between a mildly voltage-dependent pore gate (gating charge $\sim$0.18 e_o) and a voltage sensor (gating charge $\sim$1.7 e_o). The proposed voltage sensor stabilized the closing of the pore gate (coupling factor $\sim$31). We anticipate that the use of linkage analysis will broaden understanding of functional coupling in ion channels and proteins in general.

Introduction

Members of the inward rectifier (Kir) subfamily of potassium channels mediate K^+ currents, which are important in maintaining stable resting membrane potentials, controlling excitability, and shaping the final repolarization of action potentials in excitable cells such as neurons and cardiac myocytes (Noble, 1979; Constanti and Galvan, 1983; Hume and Uehara, 1985; Nichols and Lopatin, 1997; Day et al., 2005). The current–voltage relationship of Kir2.x channels displays a characteristic hump near the K^+ equilibrium potential (Matsuda et al., 1987; Vandenberg, 1987), which is attributed to the presence of a strong inward rectification mechanism, allowing inward currents to pass through the channels more easily than outward currents.

The pore of a Kir2.x channel consists of the cytoplasmic segment, central cavity, and selectivity filter. The mechanism underlying the strong inward rectification of Kir2.1 channels has been ascribed to a voltage-dependent block of outward currents by internal Mg^{2+} and polyamines (Matsuda et al., 1987; Vandenberg, 1987; Ficker et al., 1994; Lopatin et al., 1994; Stanfield et al., 1994). Outward currents through Kir2.1 channels (Kubo et al., 1993) can be inhibited by these molecules with high affinity at the central cavity or with low affinity in the cytoplasmic pore (Yang et al., 1995; Kubo and Murata, 2001).

In addition to the strong inward rectification caused by intracellular blockers, Kir2.1 channels possess "weak" inward rectification observed in inside-out patches after prolonged washout

of intracellular blockers. All currently identified prokaryotic Kir channels possess only weak inward rectification, and some eukaryotic Kir channels exhibiting weak but not strong inward rectification are involved in important physiological functions in brain, heart, kidney, pancreas, etc. (Hibino et al., 2010). A systematic comparison of prokaryotic and eukaryotic Kir channels favors the notion that strong inwardly rectifying Kir channels evolved from weakly rectifying channels (Cheng, 2012). Whether weak inward rectification observed in strongly rectifying channels subject to washout reflects the action of an evolutionarily old gating mechanism intrinsic to the channel (Lopatin et al., 1994; Yang et al., 1995; Shieh et al., 1996; Lee et al., 1999; Matsuda et al., 2003, 2010) or is an artifact of residual block (Guo and Lu, 2000; Guo et al., 2003) remains a matter of controversy.

Ion channels are activated (gated) by stimuli such as voltage and ligand binding and transduce this information into conformational changes that open/close the channel pore. One of the key questions in ion channel gating is how changes in environment lead to pore opening/closing. A working hypothesis is that specialized sensors respond to external stimuli through changes in conformation that can be transmitted to the pore gate through energetic coupling between the relevant sensors and the gate. Linkage analysis in the form of a conductance Hill plot described

[1]dPET, Spokane, WA;   [2]Institute of Biomedical Sciences, Academia Sinica, Taipei, Taiwan.

Dr. Shieh died on March 14, 2017;   Correspondence to Daniel Sigg: dansigg@gmail.com.
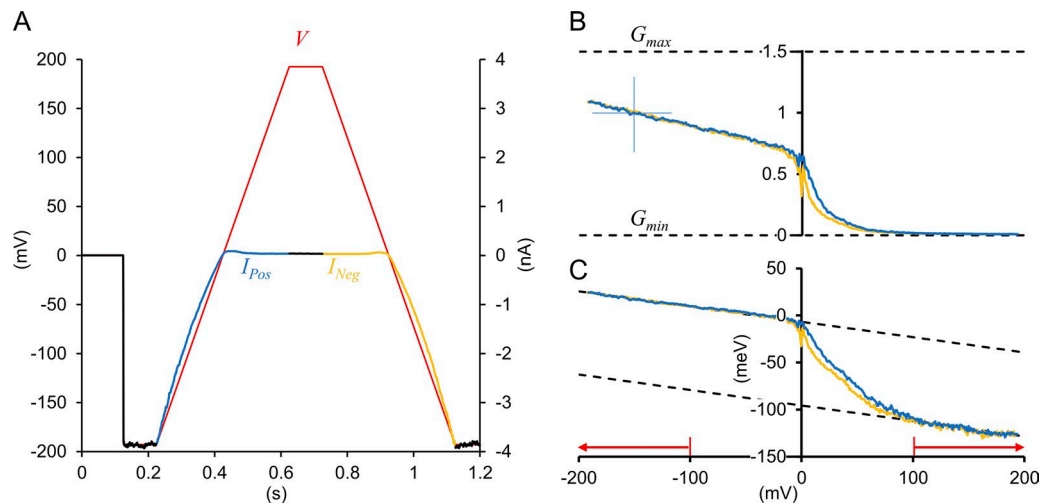
Figure 1. **Ramp protocol for recording Kir2.1 currents. (A)** Voltage protocol and current trace (experiment R1). The voltage protocol (red line) consists of a 100-ms prepulse at −200 mV, a 400-ms positive ramp (Pos) from −200 to +200 mV, a 100-ms interramp plateau phase at +200 mV, and a 400-ms negative ramp (Neg) from +200 to −200 mV. The ionic current (colored blue for Pos segment; orange for Neg segment; otherwise black) was recorded from an inside-out patch with symmetrical 20 mM [K$^+$]. **(B)** Scaled G-V curves obtained from *I-V* relationships determined from the double ramp protocol using the formula $G(V)$ = *scale* · $I(V)/(V − V_{os}) − G_{min}$ (Table 1). Ramp segments are color-coded the same as in A. **(C)** Conductance Hill plot ($W_{H[g]}$) constructed from the G-V curves in A. Red arrows demarcate the outer linear asymptotic regions used for fitting.

by $W_{H[g]}$ = $kT\ln[(G − G_{min})/(G_{max} − G)]$ versus voltage (V) can be used to describe the equilibrium relationship between pore opening (tracked by conductance G) and V-dependent modifiers of G (Chowdhury and Chanda, 2010; Sigg, 2013). The Hill plot, which has units of energy, contains one or more linear segments reflecting voltage intervals in which pore opening can be characterized by a simple two-state process. The traditional Hill approach (Hill, 1910) focuses on the region of steepest slope (Hill coefficient), which is a lower estimate for total gating charge (Yifrach, 2004). Here, we are more interested in the asymptotic behavior of the Hill plot for very large positive and negative voltages (outer segments). The vertical separation of positive-voltage and negative-voltage asymptotes in the conductance Hill plot of an allosterically regulated channel is equal to the energy of interaction between the pore and its voltage sensors. The asymptotic behavior of the Hill plot can be used to discriminate between different models of pore gating in a manner to which conventional $G(V)$ activity curves may be insensitive. In this study, we applied linkage analysis to examine various mechanisms proposed for the weak inward rectification observed in Kir2.1 channels perfused with nominal blocker-free solutions.

Materials and methods

Xenopus oocyte preparations

All surgical and anesthesia procedures have been reviewed and approved by the Academia Sinica Institutional Animal Care and Utilization Committee (Protocol 11-12-278). *Xenopus* oocytes were isolated by partial ovariectomy from a frog anesthetized with 0.1% tricaine (3-aminobenzoic acid ethyl ester). The incision was sutured, and the animal was monitored during the recovery period before it was returned to its tank. Oocytes were maintained at 18°C in Barth's solution containing (in mM): NaCl 88, KCl 1, NaHCO$_3$ 2.4, Ca(NO$_3$)$_2$ 0.3, CaCl$_2$ 0.41, MgSO$_4$ 0.82, and HEPES 15, pH 7.6, with gentamicin (20 µg/ml) and were used 1–3 d after injection of cRNA obtained from the Kir2.1 cDNA clone (Kubo et al., 1993) by in vitro transcription (mMessage mMachine, Ambion).

Electrophysiological recordings

Currents were recorded using patch-clamp techniques (Hamill et al., 1981; Hilgemann, 1995) with an Axopatch 200B amplifier (Axon Instruments). Electrodes with pipette diameters ranging from 1 to 5 µm were used. The command voltage pulses, ramp

Table 1. **Normalization and correction parameters for ramp data**

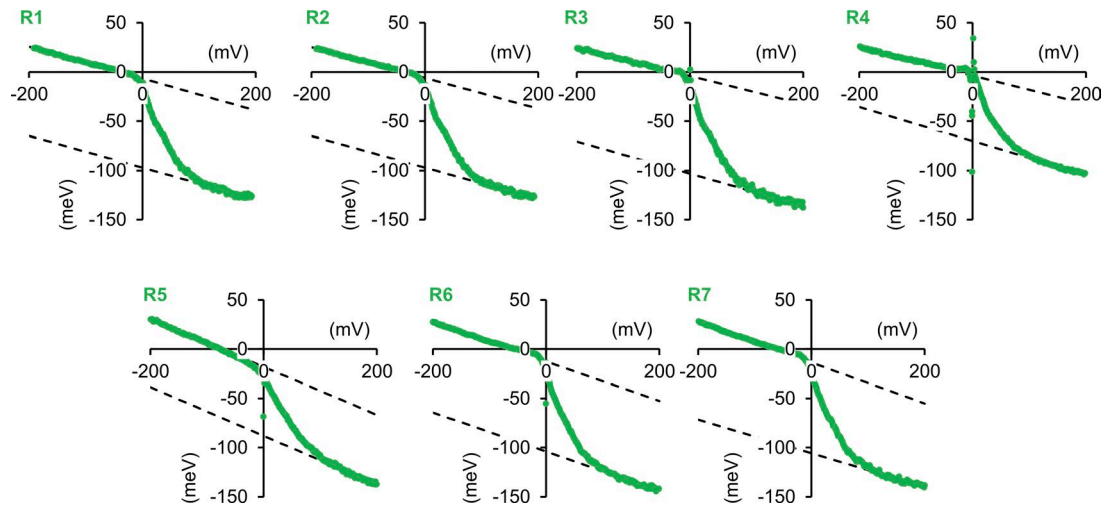| Experiment	Scale-Pos	Scale-Neg	V_{os}-Pos (mV)	V_{os}-Neg (mV)	G_{min}-Pos	G_{min}-Neg
R1	54.2	54.2	−1.4	0	0	0
R2	54.9	54.9	−1.4	0	0	0
R3	131	130	−1.0	−0.5	0.015	0.019
R4	106	105	−1.0	−1.0	0.01	0.02
R5	69.0	76.0	−0.4	−1.0	0.01	0.01
R6	40.5	40.0	−1.4	−1.0	0.0055	0.0065
R7	62.5	62.5	−1.0	−1.0	0.008	0.0095

Figure 2. **Hill plots of nominally blocker-free experiments.** Hill-transformed decimated conductance data for seven experiments (R1–R7); average of Pos and Neg traces. The dashed lines are linear regression fits to the positive-voltage and negative-voltage asymptotic regions.

protocols, and data acquisition functions were controlled using a DigiData1440 board and pClamp10 software (Molecular Devices). Sampling and filtering frequencies were 25 and 5 kHz, respectively. The currents were recorded using the inside-out patch-clamp configuration under a symmetrical bath solution composed of 14.15 mM KCl, 1 mM EDTA, 3.6 mM KOH, 1 mM K_2HPO_4, and 0.25 mM KH_2PO_4, pH 7.4. The access (series) resistances of the recording ranged between 5 and 10 MΩ and were compensated by 60–70%. All experiments were performed at room temperature ($kT \sim 25$ meV). Patches were held at 0 mV, the same as the K^+ reversal potential (V_{rev}). Any offset current was manually zeroed.

Use of ramp protocol

Because Hill plots are noisy at voltages where G approaches G_{min} or G_{max}, it was essential that ionic currents (I) be recorded for as many voltages as possible to maximize the number of data points in the $G(V)$ curve. For this purpose, we recorded currents using a slow ramp protocol. Fig. 1 A shows the ramp protocol (V) and current (I) obtained from an inside-out patch expressing Kir2.1 channels exposed to symmetrical 20 mM $[K^+]$. The ionic current demonstrated inward rectification in a nominal blocker-free solution. This inward rectification is referred to as intrinsic or weak inward rectification, to be differentiated from the "strong" inward rectification induced by polyamine or Mg^{2+} block. The subphysiological value of $[K^+]$ was chosen to reduce the size of the current for improved voltage control of the membrane patch. Symmetric $[K^+]$ values smaller than 20 mM were avoided because a low concentration of permeant ions reduced pore conductance at extreme negative potentials by an unknown mechanism.

Constructing the Hill plot

To construct a conductance Hill plot from the quasi-equilibrium $I(V)$ curve, we needed an expression for the single-channel open probability $P_O(V)$. Provided the time-averaged conductance of a channel-containing membrane has well-defined maximum and minimum values, then one can define the open probability as

$$P_0 = \frac{G - G_{min}}{G_{max} - G_{min}}. \tag{1}$$

The ionic current from N channels was assumed to have the general form $I(V, t) = g_l(V - V_l) + NP_O(V, t)g(V)(V - V_{rev})$, where the subscript l indicates an unavoidable "leak" current. Under conditions of symmetrical $[K^+]$ and after carefully zeroing the offset potential of the voltage clamp, we obtain $V_{rev} = V_l = 0$, and we set $G(V)$ equal to the chord conductance $I(V)/V = g_l + NP_O(V) g(V)$, assuming quasi-equilibrium conditions. Previous studies have shown the open-pore conductance $g(v)$ in Kir channels to be voltage independent (ohmic) in the range of –100 to 100 mV (Matsuda et al., 1987; Vandenberg, 1987). With these considerations, one obtains a sigmoidal $G(V)$ curve that is related to $P_O(V)$ through Eq. 1, after setting $G_{min} = g_L$ and $G_{max} = g_L + Ng$.

To construct Hill plots from experimental data, we plotted $G(V)$ and determined G_{min} and G_{max} so that the Hill plot was asymptotically linear for positive and negative voltages (Fig. 1, B and C). The conductance Hill energy was defined as

$$W_{H[g]} \equiv kT \ln\left(\frac{P_0}{1 - P_0}\right) = kT \ln\left(\frac{G - G_{min}}{G_{max} - G}\right). \tag{2}$$

In practice, conductance limits are better represented by $G_{min} - \varepsilon_b$ and $G_{max} + \varepsilon_a$, where ε are positive-value errors in determining G_{min} and G_{max}. As a result of these errors, which are caused by noise distortion as $G(V)$ approaches either G_{min} or G_{max}, we obtain

$$W_{H[g]} = kT \ln\left(\frac{P_0 + b}{1 - P_0 + a}\right), \tag{3}$$

where $b = \varepsilon_b/\Delta G$, $a = \varepsilon_a/\Delta G$, and $\Delta G = G_{max} - G_{min}$. An important component of Hill analysis is to minimize the proportional errors a and b, because these cause distortions in the Hill plot, clipping it in the range $kT\ln b$ to $-kT\ln a$. Only b was relevant in the present case, because $G_{max} - G$ was greater than noise for all voltages.
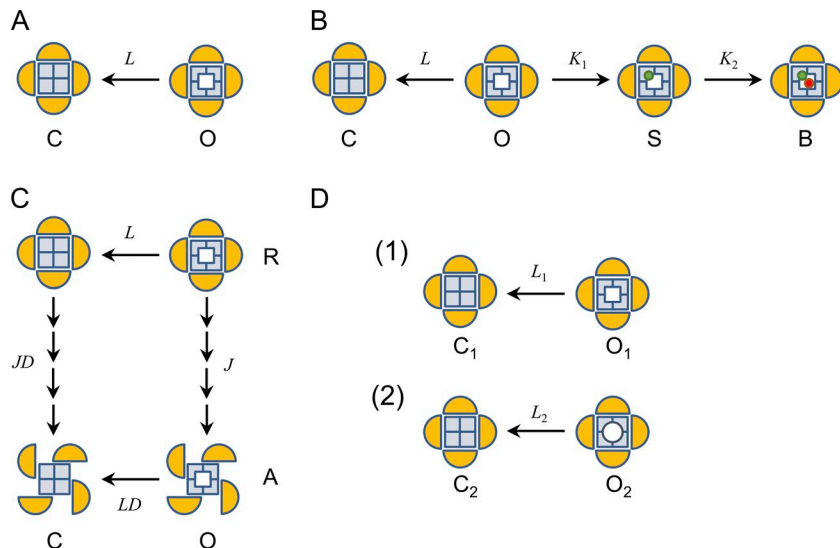
Figure 3. **Gating schemes. (A)** The C-O model. C, closed; O, open. **(B)** The COSB model. Small circles represent partial (green) and complete (red) blocking sites. **(C)** Allosteric model with four voltage-sensing J gating particles (orange half-circles). R, resting; A, activated. Intermediate configuration states are not depicted. **(D)** Two-populations model. The two pore species (1 and 2) have different conductances and gating charges.

The best estimates for G_{min} and G_{max} were obtained by requiring the Hill plot to be linear in the negative (–200 to –100 mV) and positive (+150 to +200 mV) voltage ranges. Each trace of $G(V)$ was scaled to unity at V = –150 mV (Fig. 1 B). Assigning G_{max} = 1.5 linearized the negative-voltage asymptote of the Hill plot in each of seven experiments (R1–R7, Fig. 2). In experiments R1 and R2, assigning G_{min} = 0 rendered the positive-voltage asymptote linear and parallel to the negative-voltage asymptote. Achieving linear positive-voltage asymptotes in the remaining experiments R3–R7 required G_{min} to acquire a small value in the range of 0.0065 to 0.02, presumably because of lower seal resistance or a slight current offset. A small voltage offset in the clamp apparatus (V_{os}) was corrected manually in most traces by minimizing the conductance spike at V = 0. Values for the scale factor, G_{min}, and V_{os} in each experiment are found in Table 1.

Because of time correlations in the original data, achieving statistical independence between neighboring points required reducing the original number of 4,000 (experiments R1 and R2) or 16,000 (experiments R3–R7) data points to 400, of which roughly half were in the outer segments (~100 points in each outer segment). Data reduction was performed in two ways: (1) standard decimation and (2) random sampling of the dataset with replacement (bootstrap method).

Statistical analysis

We performed least-squares fitting of various equilibrium gating schemes to the Hill plot using the solver routine in Excel (Microsoft). Only the outer asymptotic regions were included in the fit. Because the positive-voltage and negative-voltage asymptotic regions exhibited substantially different noise levels, a weighting factor equal to the inverse variance of linear regression residuals in the original (nondecimated) data was incorporated into the sum of residual squares, yielding the χ^2 statistic. Confidence intervals for fitted parameters were determined by varying the parameter of interest and determining the boundaries where χ^2 fits of the remaining parameters exceeded a critical χ^2 value corresponding to the 95% quantile of the F distribution (Kemmer and Keller, 2010). The χ^2 value was also used in model discrimination using the Akaike information criterion (AIC) score: AIC = $n\ln(\chi^2/n) + 2k$, where $n \approx 200$ is the number of independent and normally distributed data points and k is the number of fitted variables plus 1 (Horn, 1987; Burnham and Anderson, 2004; Banks and Joyner, 2017). The relative likelihood of two models describing the same dataset is given by $\exp[(AIC_1 – AIC_2)/2]$, where the smaller AIC value indicates the better model. Distributions of AIC values and fitted parameters were obtained from bootstrap-sampled data, yielding a second source of model discrimination and confidence intervals.

Equilibrium gating models

Cartoon representations of candidate gating models are shown in Fig. 3. The equilibrium properties of each model are described by their partition function Z, a Boltzmann-weighted sum of states that can be expressed as a polynomial function of equilibrium constants and allosteric factors (Sigg, 2013). The open probability P_O was obtained by multiplying each term in Z by 0 (closed) or 1 (open) or by a fractional conductance φ, and then dividing the weighted sum by Z.

The simplest scheme is the two-state gating particle (Fig. 3 A), where voltage V displaces a gating charge Δq and closes the pore. We assigned to the closing transition an equilibrium constant of the form $L = \exp(-\eta_L/kT)$. The equilibrium constant is a Boltzmann function of the transition free energy or "particle potential" given by $\eta_L = -\Delta q_L (V - V_L)$, where V_L is the half-activation potential. The partition function of the pore gating particle is $1 + L$, yielding $P_O = 1/(1 + L)$. The corresponding Hill equation is simply $W_{H[g]} = \eta_L$, which is linear with slope $-\Delta q_L$.

Residual block (COSB) model

Our previous work (Liu et al., 2012) has argued that the Kir channel contains two blocking sites, each binding one polyamine molecule, rather than progressing from partial to complete block in a singly occupied site. The resulting COSB model (Fig. 3 B) follows the scheme
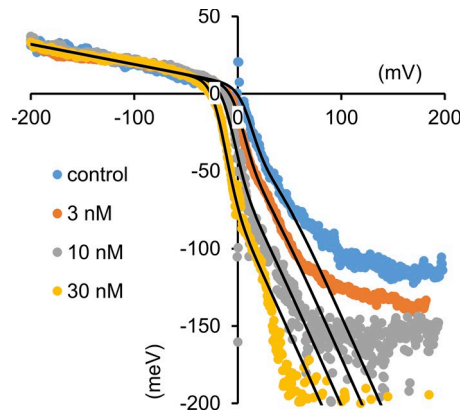
$$C \overset{L}{\leftarrow} O \overset{K_1}{\longrightarrow} S \overset{K_2}{\longrightarrow} B.$$
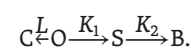
Figure 4. Hill analysis of ramp data with varying spermine concentration. Positive ramps from –200 to 200 mV with varying internal spermine concentrations from different experiments. The control experiment is nominally free of spermine. The Hill-transformed conductances were fitted by eye to the COSB model in the intermediate region around $V = 0$ mV. The G_{min} error factor b was set to zero. Adjusted variables are: $[B] = 1.0$ nM; $\Delta q_L = 0.13$ e_o, $V_L = 46$ mV, $\Delta q_1 = 3.8$ e_o, $V_1 = 8$ mV, $\Delta q_2 = 1.5$ e_o, and $V_2 = 33$ mV.

The open state is O, from which the channel may close through intrinsic pore gating (C) or undergo sequential blocking by a polyamine species, first as a partial (subconductance) block (S) by the high-affinity site, followed by complete block (B) by the low-affinity site. The arrows indicate both the direction of positive gating charge displacement and the orientation of equilibrium constants. The equilibrium constants have the following form: $L = \exp(-\eta_L/kT)$ and $K_i = \exp(-\eta_i/kT)$. The corresponding "particle potentials" are given by $\eta_L = -\Delta q_L (V - V_L)$ and $\eta_i = -\Delta q_i (V - V_i) - \mu$, where $\mu = kT\ln([B]/[B_o])$ is the chemical potential of the blocker, Δq_1 and Δq_2 are the charge displacements of partial and complete block, respectively, and V_1 and V_2 are the corresponding half-activation potentials when $[B]$ equals the standard blocker concentration $[B_o]$, which was arbitrarily assigned the value 1 nM.

The open probability for the COSB model is

$$P_O = \frac{1 + \phi K_1}{Z}, \tag{4}$$

where φ is the fractional conductance of the S state, and the partition function is $Z = 1 + L + K_1 + K_1K_2$.

The conductance Hill energy derived from Eqs. 2 and 4 is

$$W_{H[g]} = kT \ln \left[\frac{1 + \phi K_1}{L + K_1(1 - \phi + K_2)} \right]. \tag{5}$$

The asymptotic behavior of $W_{H[g]}$ at extreme voltages $(V \to \pm\infty)$ is $W_{H[g](-)} = \eta_L$ (provided $\Delta q_L < \Delta q_1$) and $W_{H[g](+)} = \eta_2 + kT\ln\varphi$ (requiring $\varphi \neq 0$, otherwise $\eta_1 + \eta_2$). The upper limit of the slope in the steepest portion of the plot (the traditional Hill coefficient) is given by $-(\Delta q_1 + \Delta q_2)$.

Allosteric model

The partition function for a radial arrangement of n voltage sensors J around a single pore L is: $Z = (1 + J)^n + L(1 + JD)^n$, where L and J are voltage-dependent equilibrium constants: $L = \exp(-\eta_L/kT)$ and $J = \exp(-\eta_J/kT)$, whose particle potentials are given by

$\eta_X = -\Delta q_X (V - V_X)$. The state diagram is shown in Fig. 3 C. The coupling factor is $D = \exp(-\eta_D/kT)$, where $\eta_D = W_D - \Delta q_DV$, and W_D is the interaction energy. The open probability is $P_O = (1+J)^n/Z$. The conductance Hill energy is $W_{H[g]} = \eta_L + nkT\ln[(1 + J)/(1 + JD)]$, with asymptotes $W_{H[g](-)} = \eta_L$ and $W_{H[g](+)} = \eta_L + n\eta_D$. Thus nW_D is the vertical separation between positive and negative asymptotes at $V = 0$. The upper limit of the slope at intermediate voltages is $-(\Delta q_L + n\Delta q_J + n\Delta q_D)$.

Two-populations model

The partition function for the sum of independent pore particles is $Z = (1 + L_1)^{N1}(1 + L_2)^{N2}$, where the two populations N_1 and N_2 satisfy $N_1 + N_2 = N$, and the pore equilibrium constants L_1 and L_2 are voltage dependent. The model scheme (Fig. 3 D) invokes two populations of channels with weakly voltage-rectifying pores (gating charges Δq_1 and Δq_2) and possibly distinct conductance values g_1 and g_2. Setting population fractions to $f_1 = N_1g_1/(N_1g_1 + N_2g_2)$ and $f_2 = 1 - f_1$, we can write the open probability as

$$P_O = \frac{\langle g \rangle}{g_{\max}} = \frac{f_1}{1 + L_1} + \frac{f_2}{1 + L_2}. \tag{6}$$

As usual, $W_{H[g]} = kT\ln[P_O/(1 - P_O)]$. The channel populations are pure if f_1 equals 0 or 1. In such cases, we obtain straight lines for the Hill plots corresponding to either η_1 or η_2. The asymptotic behavior for intermediate f values depends on which species carries the lesser charge:

$$W_{H[g](-)} = \begin{cases} \eta_1 - kT\ln f_1 & \text{if } \Delta q_2 > \Delta q_1 \\ \eta_2 - kT\ln f_2 & \text{if } \Delta q_1 > \Delta q_2 \end{cases}, \tag{7}$$

$$W_{H[g](+)} = \begin{cases} \eta_1 + kT\ln f_1 & \text{if } \Delta q_2 > \Delta q_1 \\ \eta_2 + kT\ln f_2 & \text{if } \Delta q_1 > \Delta q_2 \end{cases}. \tag{8}$$

The "interaction energy" is equal to $2kT\ln f_1$ or $2kT\ln f_2$, but this is a fictitious quantity, as there is no energy linkage between the two channel species. When the charges of the two populations are of similar value, the result is essentially a straight-line Hill plot with slope $\Delta q_1 \approx \Delta q_2$.

Kinetic analysis

Berkeley Madonna (Macey and Oster) was used to solve the kinetics of the equivalent circuit model using a fourth-order Runge–Kutta algorithm. It was also used for least-squares fitting of kinetic parameters in the equivalent circuit model.

Results

Comparing proposed mechanisms of weak inward rectification

Previous studies have suggested that blocker-free inward rectification is caused by a weakly charged gating transition (Matsuda et al., 2003, 2010). In a two-state C-O scheme, the theoretical Hill plot is a straight line with slope equal to Δq_L, the gating charge of the pore gate. However, the experimental Hill plots are consistently sigmoidal (Fig. 2), suggesting that in nominal blocker-free solutions the pore gate is coupled to a second voltage-dependent process.

We considered whether the second process could be a blocking event. First, we postulated that incompletely washed polyamines
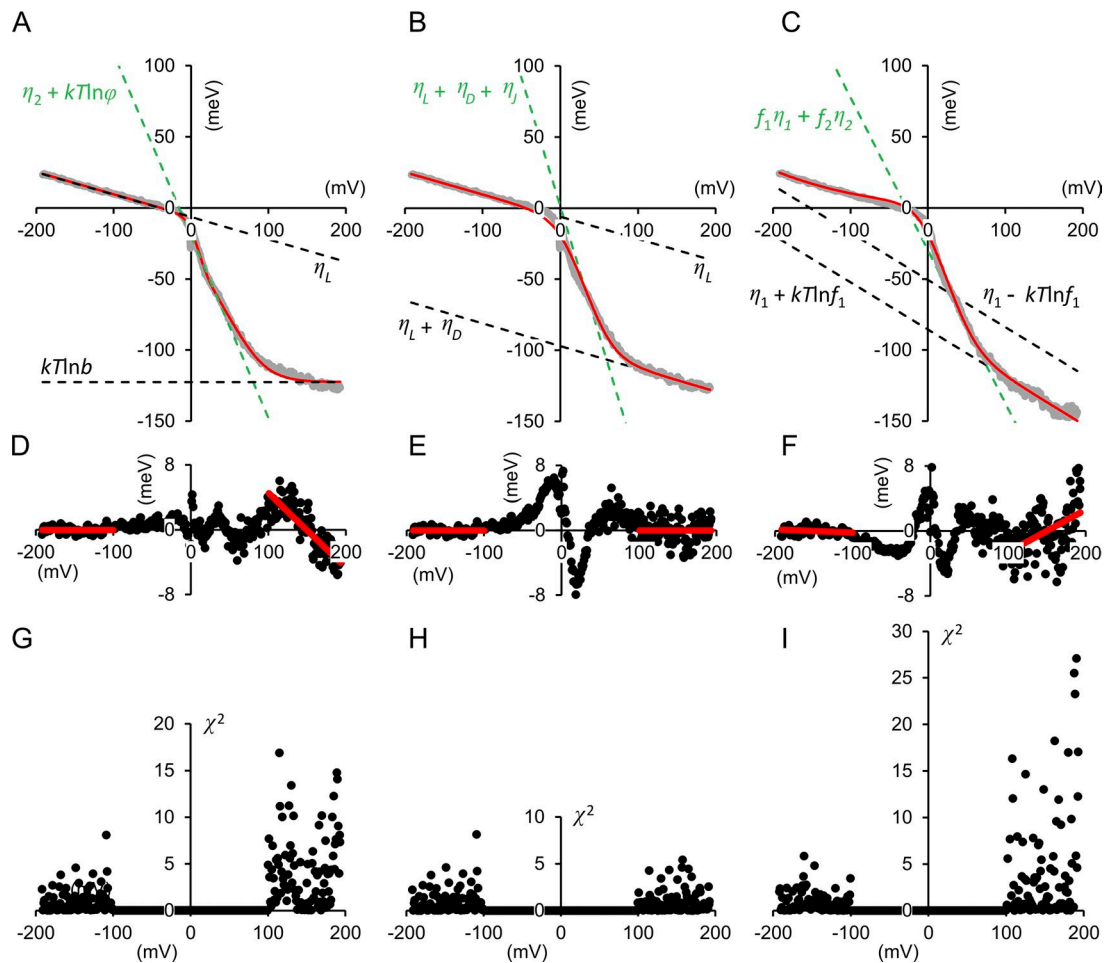
Figure 5. Fits of blocker-free gating models to the Hill plot. Experiment R2. The experimental Hill plot is in gray, whereas fitted lines are solid red. Linear asymptotic regions are designated by black (shallow outer segments) or green (steeper intermediate region) dashed lines, accompanied by the model-specific formula that describes them. **(A)** The COSB model. The value of φ was set to 0.2 as previously established (Liu et al., 2012). Fitted parameters were: $\Delta q_L = 0.16$ e_o; $V_L = -41$ mV; $\Delta q_{K1} = 3.49$ e_o; $V_{K1} = 1.58$ mV; $\Delta q_{K2} = 1.28$ e_o; $V_{K2} = 20.3$ mV; $b = 0.0074$. The COSB model predicts that the blocking transition S→B should be represented by a steep positive asymptote with limiting slope Δq_{K2} (dashed green line). However, to more closely fit the data, the positive-voltage asymptote was clipped at the value of $kT\ln b$ (lower dashed black line). **(B)** Allosteric scheme ($n = 1$). The shallow upper and lower extreme asymptotes are functions of the pore sensor L and the strength of its interaction with J, whereas the steeper intermediate slope (Hill coefficient) is a lower limit for the total gating charge dominated by the J particle. The very small difference in slope between the shallow asymptotes reflects a tiny coupling charge ($\Delta q_D = 0.003$ e_o). $\Delta q_L = 0.16$ e_o; $V_L = -39$ mV; $\Delta q_J = 1.65$ e_o; $V_J = 60$ mV; $W_D = -91$ meV (-2.1 kcal/mol). **(C)** The two-population model. The common slope of the two shallow asymptotes reflects gating in the channel with the smaller gating charge (channel 1). The steeper intermediate slope is the weighted mean of particle potentials from both channels. $\Delta q_{L1} = 0.33$ e_o, $V_{L1} = -205$ mV, $\Delta q_{L2} = 1.81$ e_o, $V_{L2} = 4$ mV; $f_1 = 0.50$. **(D–F)** Residuals from least-squares fit. Linear regression lines for the residuals at the outer asymptotic regions are in red. Residuals points were normally distributed around their regression line (P value range: 0.49–0.99, Shapiro–Wilk test). The slopes of the outer residuals in the allosteric model, and in the Neg residual of the COSB model, are statistically equal to zero (P = 0.99, F test). However, nonzero slopes in the residuals are found in the Pos asymptotes of the COSB and two-populations model (P < 0.001) and in the Neg asymptote of the two-populations model (P = 0.02). **(G–I)** χ^2 values used in the fit statistic, with inverse weights 0.148 meV^2 (Neg) and 2.12 meV^2 (Pos), equal to the variances calculated from residuals in the nondecimated data.

are responsible for inward rectification. Our previous study (Liu et al., 2012) suggested that spermidine block can be described by the four-state COSB model, where S is a subconducting state induced by high-affinity polyamine block and B is the completely blocked state attributed to low-affinity binding. To estimate the amount of residual spermine necessary to account for the observed rectification, it was necessary to perform ramp experiments with varying spermine concentrations plus a nominally blocker-free control (Fig. 4) and fit the COSB model to the corresponding Hill-transformed conductance curves. The control plot was compatible with a residual spermine concentration of

1.0 nM, which was applied to subsequent fits of the COSB model to nominally blocker-free experiments. The negative-voltage asymptote corresponding to the closing transition ($\Delta q_L = 0.18$ e_o) was well represented by the model, but the positive-voltage asymptote is predicted to be steeper, with slope equal to the charge displacement of the low-affinity blocker (Fig. 4, black lines, $\Delta q_2 = 1.5$ e_o; Fig. 5 A, green dashed line, $\Delta q_2 = 1.1$ e_o). By considering the possibility of a G_{min} baseline error, we forced the positive asymptote to level off at the value $kT\ln b$. The same behavior occurs if the B state demonstrates partial block. However, the clipped curve produced a downward sloping residual in the positive-volt-
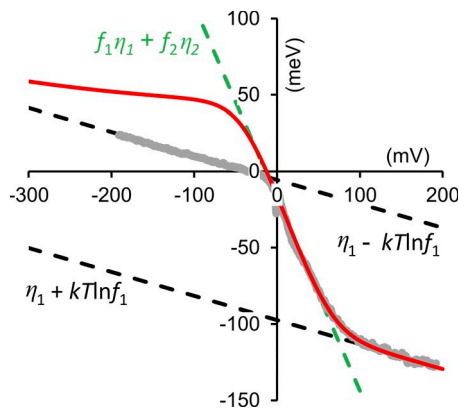
Figure 6. Fit of two-population model assuming $\Delta q_1 = \Delta qL$. Data same as in Fig. 4. Fitted variables are $\Delta q_1 = 0.16\ e_o$, $V_1 = -328$ mV, $\Delta q_2 = 1.47\ e_o$, $V_2 = -8$ mV; $f_1 = 0.16$.

age linear asymptote of the Hill plot (Fig. 5 D), resulting in a poor fit. Thus incomplete polyamine washout is not compatible with weak inward rectification. Parameter values for the COSB model obtained from seven experiments are listed in Table 2.

After evaluating blocking mechanisms, we considered allosteric interactions between a weakly voltage-dependent pore region and a second voltage sensor. The allosteric model fit the Hill plot well in the critical outer asymptotic regions (Fig. 5 B). Like the COSB model, the allosteric model predicted a small gating charge of pore opening ($\Delta q_L = 0.18\ e_o$; Table 3). The value of Δq_D (= $0.002\ e_o$) was not statistically different from zero (P = 0.80, Student's t test), implying no difference in the slopes of the positive and negative voltage asymptotes. The proposed voltage sensor J demonstrated a voltage sensitivity ($\Delta q_J = 1.65\ e_o$) larger than the pore by an order of magnitude. The interaction energy between the two processes was computed to be $W_D = -86$ meV (−2.0 kcal/mol), equating to a coupling factor of $D = 31$. Because Kir channels contain four subunits, we considered the interaction of the pore with $n = 4$ identical voltage sensors. The resulting five-particle model had no effect on the outer asymptotic regions, nor did it significantly improve the fit in the intermediate region around $V = 0$, where residuals from the COSB model are found to be smaller (Fig. 5, D and E). The intermediate region of the Hill

plot was more accurately described by the allosteric model with the addition of a second transition to the J particle, resulting in a six-state scheme with three additional parameters. However, since the experiments were designed to measure the outer asymptotic segments and hysteresis and voltage-offset artifacts can produce distortions in the steep intermediate portion of the curve, we decided that pursuing a better overall fit did not warrant the added complexity of the six-state model.

Finally, we explored whether the sigmoidicity of the Hill plot can be attributed to independent populations of simple two-state channels (Ishihara and Ehara, 2004). This scenario corresponds to the traditional method of fitting equilibrium curves to a sum of s Boltzmann curves, where in this case $s = 2$. In principle, the lesser charge movement (Δq_1) should equal the slopes of the two outer segment asymptotes, as is the case for the allosteric model. The vertical displacement between the asymptotes is a function of the fraction of channels with the smaller charge (f_1). Equating the asymptotic slopes of the allosteric and two-populations models ($\Delta q_1 = \Delta q_L$), one obtains a value of $f_1 = 0.16$, comparable to estimates between 0.1 and 0.25 from previous work performed in the presence of polyamines (Ishihara and Ehara, 2004). However, this created a sizeable hump as the curve attempted to reach the negative-voltage asymptote after overreaching (Fig. 6). A better match of the theoretical curve to the experimental Hill plot required a larger asymptotic slope ($\Delta q_1 = 0.34\ e_o$), which led to a more balanced distribution of channel populations ($f_1 = 0.51$; Fig. 5 C and Table 4). However, these parameter adjustments came at a cost, because the slopes of the outer asymptotic segments did not match the experimental Hill plots as well as the allosteric model (Fig. 5 F). Regression analysis of residuals in all seven experiments for the two-populations model demonstrated nonzero slopes in the positive-voltage asymptote (P values from 5×10^{-7} to 0.24, F test), though less compellingly so in the negative-voltage asymptote (P values from 0.02 to 0.38). The same analysis applied to the allosteric model convincingly failed to demonstrate a nonzero residual slope in either the positive-voltage (P values from 0.79 to 0.99) or negative-voltage (P values from 0.92 to 0.99) asymptotes.

Ranking models with AIC scores
To supplement the above considerations, the three models were ranked according to their AIC score, which awards parsimony

Table 2. Fit parameters for COSB model ($n = 7$)

Particle or interaction	Parameters	Values (mean ± SEM)
Pore (L)	Δq_L (e_o)	0.18 ± 0.01
	V_L (mV)	−50 ± 7
Binding site (K_1)	Δq_1 (e_o)	3.4 ± 0.4
	V_1 (mV)	3 ± 1
Binding site (K_2)	Δq_2 (e_o)	1.10 ± 0.08
	V_2 (mV)	12 ± 4
Blocker concentration	$[B]$ (nM)	1.0 [fixed]
Fractional conductance	ϕ	0.2 [fixed]
G_{min} error factor	b	0.007 ± 0.002

Table 3. Fit parameters for blocker-free allosteric model ($n = 7$)

Particle or interaction	Parameters	Values (mean ± SEM)
Pore (L)	Δq_L (e_o)	0.18 ± 0.01
	V_L (mV)	−48 ± 7
Voltage sensor (J)	Δq_J (e_o)	1.65 ± 0.07
	V_J (mV)	57 ± 2
	n	1 [fixed]
L-J coupling	Δq_D (e_o)	0.002 ± 0.008
	W_D (meV)	−86 ± 5
	W_D (kcal/mol)	−2.0 ± 0.1
	$D\ (V = 0)$	31

Table 4. **Fit parameters for two-populations model (*n* = 7)**

Particle or interaction	Parameters	Values (mean ± SEM)
Pore 1	Δq_1 (e$_o$)	0.34 ± 0.02
	V_1 (mV)	−199 ± 6
Pore 2	Δq_2 (e$_o$)	1.71 ± 0.08
	V_2 (mV)	2 ± 2
Pore 1 fraction	f_1	0.51 ± 0.01
G_{min} adjustment	ΔG_{min}	0.005 ± 0.001

by yielding lower scores for smaller numbers of adjustable variables. Because only the outer asymptotic regions are reliably measured by the slow ramp experiment, the χ^2 value used for AIC scoring included these regions only (Fig. 5, G–I), and only the variables that affect the outer asymptotes of the Hill plot were used in the fitting process; specifically Δq_L, V_L, W, and Δq_D for the allosteric model (k = 5), Δq_L, V_L, and b for the COSB model (k = 4); and Δq_1, V_1, f_1, and ΔG_{min} for the two-populations model (k = 5). AIC scores were consistently lower for the allosteric model across all experiments, whereas the COSB and two-populations models received similar scores, with the exception of experiment R4, where the two-populations model ranked higher (Fig. 7).

Comparing variation of fitted parameters across experiments

To assess the reliability of fitted parameters across experiments, we obtained confidence intervals for the adjustable parameters fitted to the outer asymptotes (Fig. 8), using the critical χ^2 method in the case of the decimated data, and measuring variability in parameter estimates from the bootstrap-sampled data. In order for the two methods to be comparable, the bootstrap estimates used standard deviations, and so were $\sqrt{n}$-fold larger than confidence intervals of the mean, which is based on standard errors. The means and confidence intervals of adjustable parameters across all gating schemes and experiments are plotted in Fig. 9. In all variables analyzed, there was greater variability

in their fitted values across experiments than within individual experiments (P < 0.001, ANOVA). However, parameter estimates tended to be more closely correlated when performed on oocytes from the same frog. This is was the case for grouped experiments [R1, R2] and [R6, R7], each of which were performed in one day, though not for the group [R3–R5], which was performed in the span of a week.

Kinetic models

The Hill plot is an equilibrium curve, and therefore there is the possibility that the dynamic ramps used in our experiments violate the quasi-equilibrium condition. There are two sources of error. First, series resistance in the pipette (5–10 MΩ) combined with large inward currents (>1 nA) can decrease the magnitude of the effective membrane potential in a time- and voltage-dependent manner, potentially causing nonlinearity in the negative voltage segment of the Hill plot. Second, the ramp speed, although fairly slow (1 mV/ms), produces a time delay in the dynamic G-V curves compared with the true equilibrium curves. The reason for the double ramp protocol was to evaluate the time delay, which appears as a small hysteresis between the positive (Pos) and negative (Neg) curves at the steepest portion of the Hill plot (Fig. 1 C), where gating processes are characteristically at their slowest.

To test for these errors, we used kinetic modeling with an equivalent circuit (Fig. 10 A) that was able to account for the effects of membrane capacitance, series resistance, and membrane leak on the ramped current. We used a dynamic formulation of the n = 1 allosteric model (Fig. 10 B), which is shown here to fit the Hill plot well in its equilibrium form. The equivalent circuit model adequately accounted for the passive membrane components before and after capacity and series resistance compensation (Fig. 10, C and D). The distortions of the ionic current and membrane potential were minor even though the maximum current approached 4 nA (Fig. 10 E). The gating parameters for the kinetic model that aimed to reproduce the hysteresis in the Hill curves were very similar to those obtained assuming true
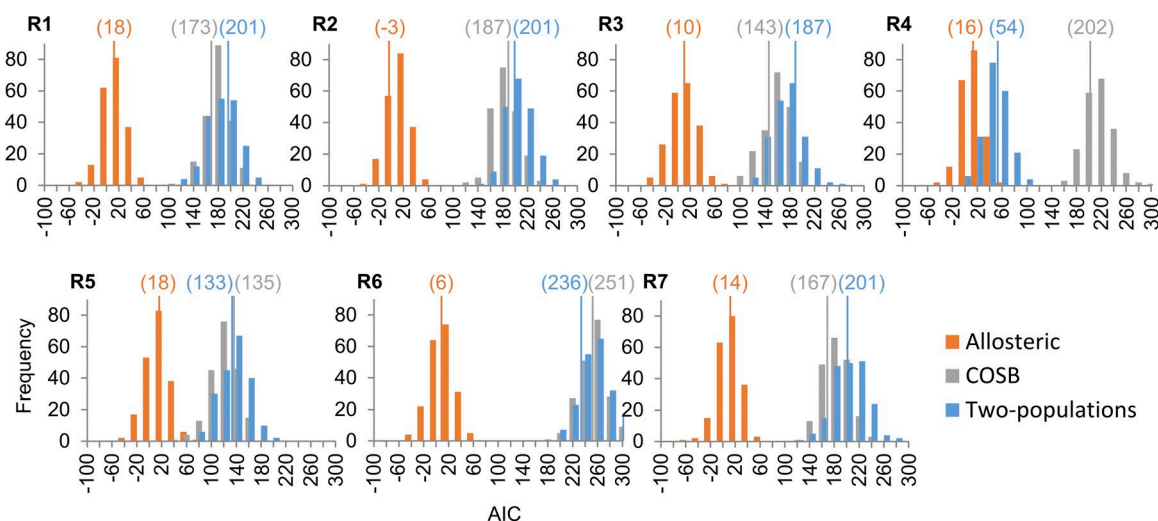

Figure 7. **AIC analysis.** Histogram of bootstrap AIC scores for three candidate models in experiments R1–R7. The AIC scores obtained from decimated tracings are indicated by thin vertical lines whose values are shown in parentheses.
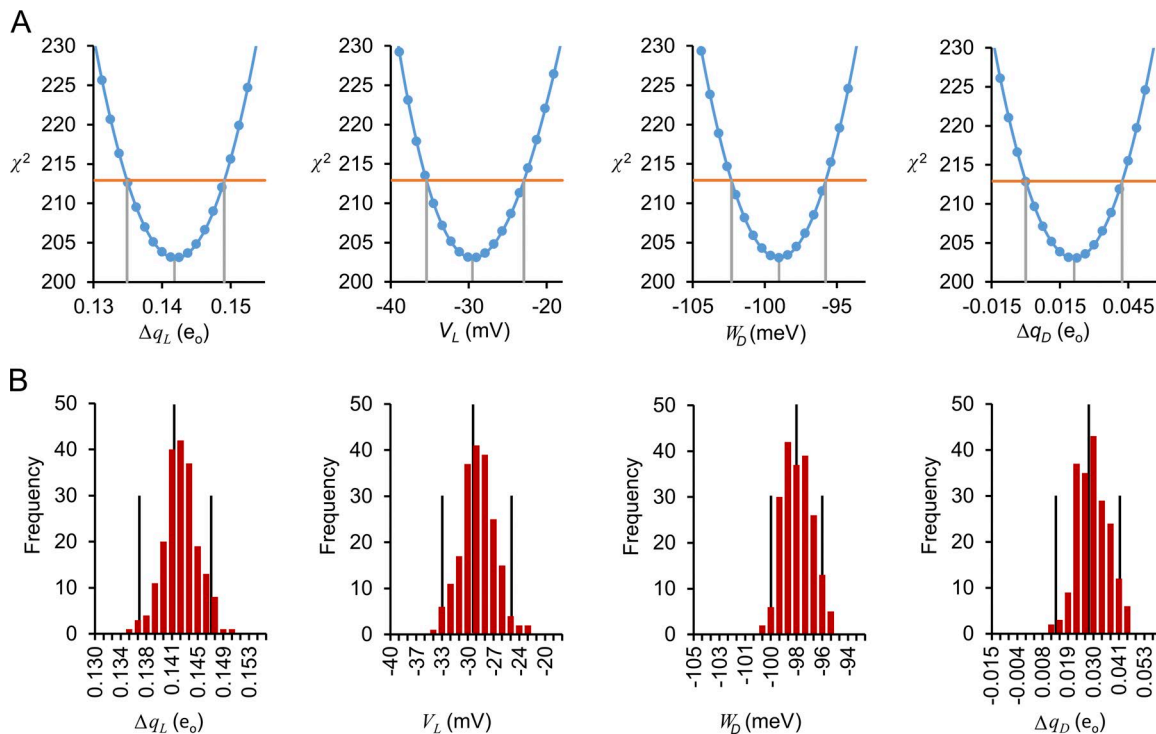
Figure 8. **Confidence intervals for allosteric model parameters in a single experiment (R3). (A)** χ^2 values plotted against the variable of interest (x) are obtained by fitting the remaining variables to the decimated data set while keeping x fixed The critical χ^2 value (horizontal orange line) for 95% confidence intervals was obtained from the F distribution: $\chi^2_{crit} = \chi^2_{min} \{1 + [m/(n - m)]F(0.05, m, n - m)\}$, where χ^2_{min} is obtained from fitting all variables, n is the number of data points, and m is the number of adjustable parameters (Kemmer and Keller, 2010). In the particular case of the allosteric model shown here, $m = 4$ (Δq_L, V_L, W_D, Δq_D). The variables that determine the steep intermediate portion of the Hill plot ($\Delta q_J = 1.67\ e_o$; $V_J = 61.9\ mV$) were kept constant. The mean and lower and upper confidence limits are indicated by the vertical gray lines. **(B)** Distributions of parameter values from 200 bootstrap samples. Mean values μ and 95% confidence intervals are indicated by vertical black lines. Confidence intervals were determined from μ ± 1.96σ, where σ is the sample standard deviation.

equilibrium (Fig. 10 F). These results show that the ramp protocol is suitable for obtaining quasi-equilibrium G-V relationships, particularly at extreme voltages where the Hill plot is expected to be linear and the system equilibrates rapidly.

Discussion

Weak inward rectification of Kir channels plays an important physiological function in many organs including brain, heart, kidney, and pancreas (Hibino et al., 2010). However, the underlying mechanism remains elusive. The purpose of this study was to systematically investigate candidate hypotheses through the use of Hill analysis, which can resolve cooperative models of gating by emphasizing their asymptotic behavior at extreme voltages. Detailed analysis suggested that the intrinsic inward rectification is caused by the allosteric coupling between a very weakly voltage-dependent pore gate ($\Delta q_L \sim 0.18\ e_o$) and a voltage sensor with roughly 10-fold greater gating charge ($\Delta q_J \sim 1.7\ e_o$). A positive coupling factor ($D \sim 31$) between the two gating particles suggests that voltage gating stabilizes the closing of the channel. Hill analysis determined that neither a simple pore gate nor residual polyamine block could account for the weak inward rectification. A simple pore gate would generate a straight-line Hill plot, whereas the lower asymptote for any blocker model such as the COSB model would be steep, reflecting the charge carried by the blocker molecule. On the other hand, the two-populations

model, like the allosteric model, is compatible with parallel outer segment asymptotes, but a pronounced hump in the region of $V < 0$ predicted by the two-populations model was incompatible with the experimental data (Fig. 6). A previous study (Ishihara and Ehara, 2004) examining the two-populations model in the presence of polyamines would not have resolved the hump, because they measured $\ln(G/G_{max})$ rather than $\ln[G/(G_{max} - G)]$. The former is sensitive only to the positive-voltage asymptote. To prevent the hump, the lesser of two gating charges needed to be increased from ~0.18 to ~0.34 e_o, which required an adjustment to G_{min} and an increase of the population fraction f_1 from ~0.16 to ~0.51. Even with these parameter changes, the fit failed to match the slope of the outer asymptotic segments of the Hill plot as well as the allosteric model (Fig. 5, E and F). In short, the demonstration of a sigmoidal transition between equally shallow linear asymptotes separated by a coupling energy is most naturally explained by a two-particle allosteric scheme, a conclusion supported by AIC ranking of the models (Fig. 7).

Most Kir channels possess weak inward rectification in nominal blocker-free solutions. The weak inward rectification in Kir2.1 has been explained by voltage block of residual polyamines or contaminates in solutions (Guo and Lu, 2000; Guo et al., 2003). However, previous studies have shown that extensive washout of inside-out patches with Mg^{2+}- and polyamine-free solutions could not remove the weak inward rectification (Vandenberg, 1987; Kubo et al., 1993; Shieh et al., 1996; Omori et al., 1997; Oishi
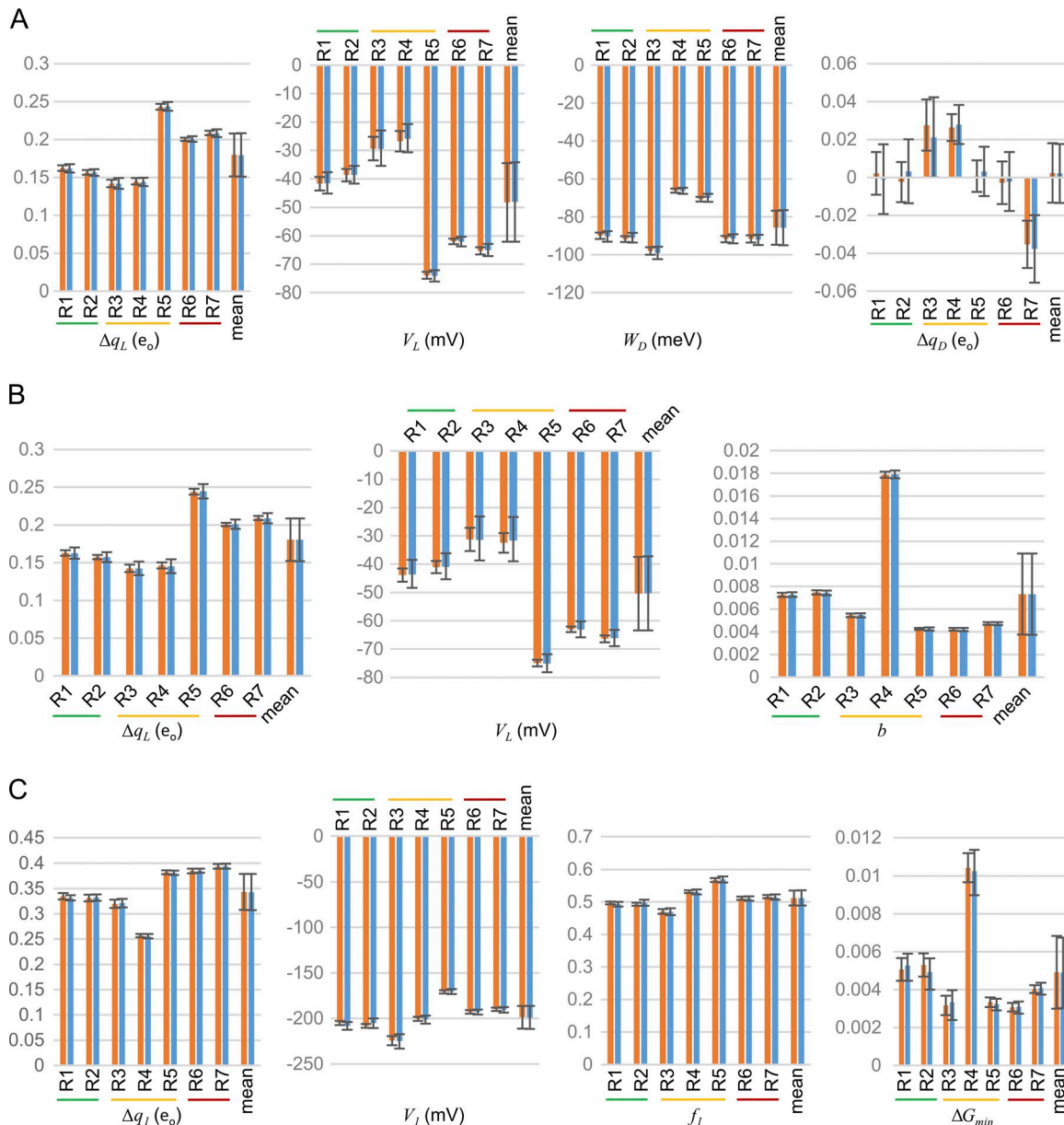
Figure 9. **Mean parameter values and confidence intervals for all experiments.** Same procedure described in Fig. 8, applied to all experiments and gating schemes. Blue columns, decimated data; orange columns, bootstrap sampled data. **(A)** Allosteric model. **(B)** COSB model. **(C)** Two-populations model. Error bars indicate 95% confidence intervals. Columns labeled "mean" represent the overall mean and 95% confidence intervals from individual means in experiments R1–R7. Colored horizontal lines indicate which experiments were performed on oocytes from the same frog.

et al., 1998; Matsuda et al., 2003, 2010; Ishihara and Ehara, 2004). A blocker model lacking the voltage sensor would require consistent trace levels of "residual" blocking ion concentration, which would be difficult to control and would generate Hill plots of varying depth. In this study, fits of the COSB model to conductance Hill plots with known spermine concentrations were compatible with a residual spermine concentration of 1.0 nM for nominally blocker-free preparations (Fig. 4), a larger value than previous upper limits for residual spermine concentrations (0.1 to 0.5 nM; Matsuda et al., 2003; Liu et al., 2011). It is unlikely that washout after pipette excision from the oocyte would yield consistent levels of residual polyamine levels at this concentration. One can generalize this result to any gating process relying on internal polyamine blockers. For example, allosteric interaction between one or more polyamine binding sites and the pore would successfully model the outer asymptotes, but would require a residual polyamine presence. Such an allosteric scheme would also require 1 mM residual spermine, because for a given Δq, the horizontal spacing between curves at intermediate voltages is uniform for constant ratios between spermine concentrations, and the analysis in Fig. 4 applied to the COSB model would also apply in this case.

The nature of the putative voltage sensor J coupled to the pore is unclear, as the Kir channel lacks a canonical voltage sensor. One possibility is that one or more permeant ions bind to sites within the pore (Kurata et al., 2010; Schewe et al., 2016). Given
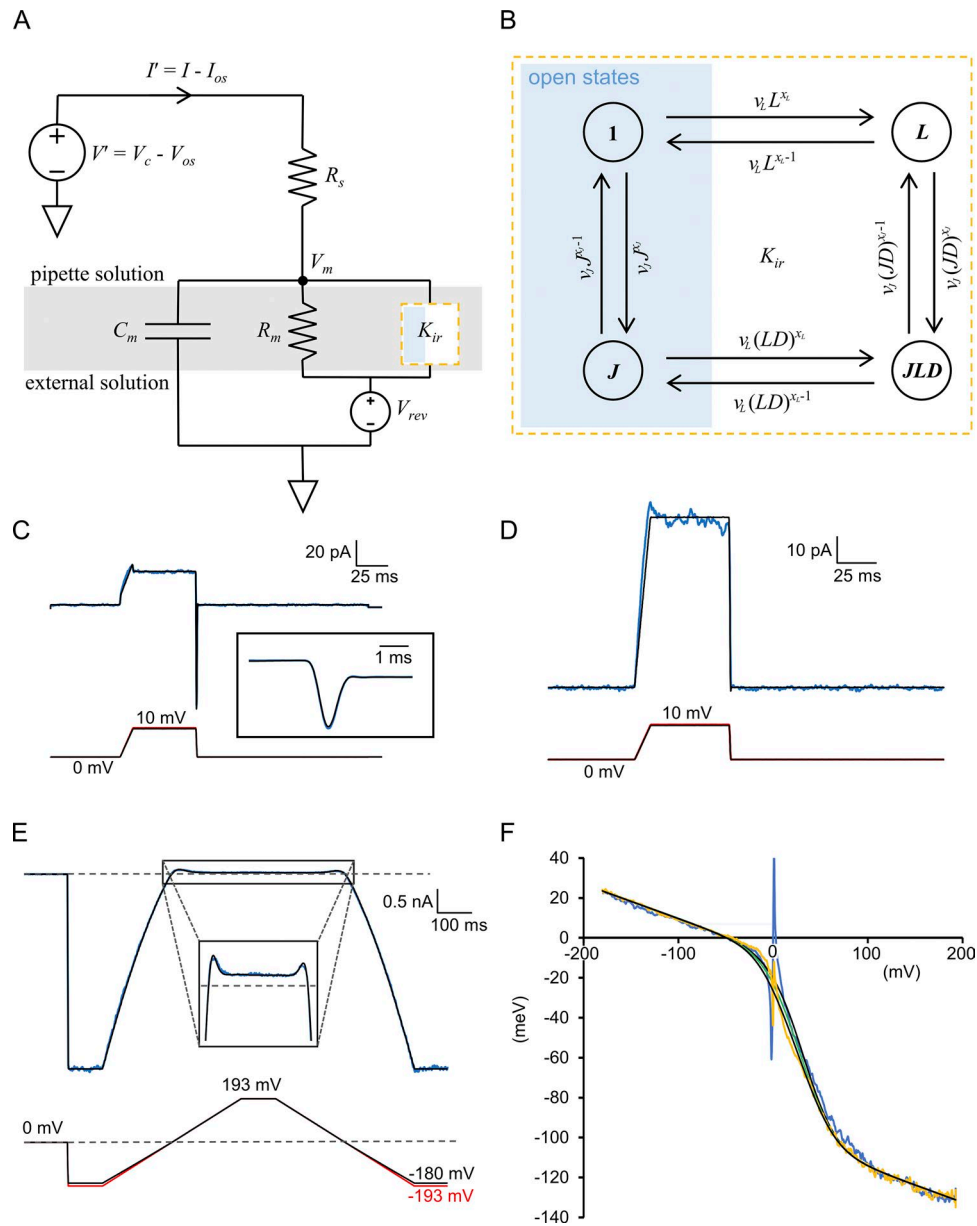
Figure 10. Equivalent circuit and kinetic model. (A) Patch-clamp elements. V_c, command potential; V_{os}, voltage offset; I, membrane current; I_{os}, current offset; R_s, series resistance; V_m, membrane potential; V_{rev}, reversal potential (assigned zero for symmetric solutions); C_m, membrane capacitance; R_m, leak resistance. The governing equation is $I' = (V' - V_m)/R_s = C_m(dV_m/dt) + G(V_m - V_{rev})$, solved numerically for V_m with initial conditions $V_m(0) = V'(0)/(1 + R_s/R_m)$. The membrane conductance G is given by $G_{min} + P_o(G_{max} - G_{min})$, where P_o is open probability, $G_{min} = 1/R_m$, and $G_{max} - G_{min} = Ng_L$ (product of channel number and unit conductance). **(B)** Kinetic scheme for the $n = 1$ allosteric model of Kir. The four states are labeled according to their contribution to the partition function. Expressions for rate constants are shown next to transition arrows. Ratios of forward to backward rate constants simplify to one of these transition equilibrium constants: L, J, LD, or JD, which also equal to the ratio of product to reactant terms in the partition function. Prefactors v_L and v_J are transition frequencies for the L and J particles, respectively. The linear free energy variables x_L and x_J range from 0 to 1. State probabilities were calculated by numerically integrating the rate differential equations governing the model using V_m as input, with initial conditions determined by the starting equilibrium distribution. **(C)** Newly formed inside-out patch without leak, capacity, or series resistance compensation (experiment R1). A fit (black line) of the ionic current (blue) to the linear elements of the equivalent circuit yielded $R_s = 10.9$ Mohm and $C_m = 7.33$ pF. The "leak" current contains contributions from both R_m and channel openings. The inset shows an expanded view of the inward capacity transient. The voltage protocol is shown at the bottom (red, V_c; black, V_m). $V_{os} = -0.04$ mV; $I_{os} = 0.0019$ pA. **(D)** Same patch as in C, but after capacity and 70% series resistance compensation. Equivalent circuit parameters were changed to $R_s = 3.23$ Mohm, $C_m = 1.0$ pF. Same patch subject to double ramp protocol. Experimental recordings of membrane current I and command voltage V_c are in blue and red, respectively. Dashed horizontal lines indicate zero values for current and voltage tracings. The inset is an enlargement of the current at very positive voltages. The black lines represent calculations of I and V_m using simultaneously equivalent circuit and gating models in response to V_c with adjustable variables derived from the Kir kinetic model and simultaneously fitted to I and the Hill plot. $I_{os} = -0.00074$ pA; $V_{os} = 0$ mV. R_s and C_m, same as in D. **(F)** Hill plots derived from Pos (blue) and Neg (orange) ramp currents, showing mild hysteresis. The black lines are the dynamic fits. The center green line is the calculated equilibrium Hill energy. Model variables: $Ng_L = 30$ nS; $\Delta q_L = 0.17$ e$_o$; $V_L = -44$ mV; $v_L = 2.0$ kHz; $x_L = 0.2$; $\Delta q_J = 1.69$ e$_o$; $V_J = 55$ mV; $v_J = 0.15$ kHz; $x_J = 0.65$; $W_D = -90$ meV (-2.1 kcal/mol).

that $\Delta q_J = 1.7$ e$_o$, at least two monovalent or one ion divalent species would need to travel nearly the entire distance of the electric field to behave as the voltage sensor, although the distance requirement might be divided by four if voltage-sensing duties were split among the four subunits. We saw no improvement in fitting with a single J particle versus four J particles; however, our experiments were not designed to accurately define the steep intermediate portion of the Hill curve. With permeation-type gating, one expects the half-activation voltage V_J to depend on the concentration of the contributing ion species. The modulation of Kir gating by permeant K$^+$ has long been recognized (Hagiwara et al., 1976), and it is conceivable that J "particle" activation represents the voltage-dependent unbinding of K$^+$ from one or more sites within the protein to the extracellular solution. The particle potential describing such an event is $-\Delta q_J (V - V_J)$, where the half-action potential $V_J ([\Delta W_J + \mu_o]/\Delta q_J)$ increases with increasing chemical potential $\mu_o = kT\ln[K^+]_o$ of the external ion, consistent with an observed rightward shift in outward current with increasing $[K^+]_o$ (Chang et al., 2010). Although a permeation-type gating mechanism is plausible given the importance of blockers and permeant ions in Kir gating, one cannot rule out that charged protein residues located within one of the transmembrane domains could be collectively acting as a voltage sensor. Potential candidates include K182 in the C-terminal portion of the M2 domain, R148 located just two residues beyond the highly conserved GYG sequence in the selectivity filter, D172 in the midportion of the M2 domain (known to be a polyamine binding site), and E138 in the midpore domain. Charge-neutralization experiments (Aggarwal and MacKinnon, 1996; Seoh et al., 1996) would be necessary to determine whether fixed charges contribute to voltage sensing in the blocker-free channel.

Constructing the conductance Hill plot required accurate measurements of channel open probability (Eq. 1). Previous studies (Horrigan et al., 1999; Islas and Sigworth, 1999; González-Pérez et al., 2010) have determined the limiting conductance slope from a series of constant-voltage conductance histograms (NPo method), but the technique is not suitable for very large currents when $Po \approx 1$, so we used the ramp approach, which had the advantage of sampling all voltages in a single trace. A limitation of this study is the potential errors in determining G_{min} and G_{max}. It was not possible to unambiguously measure the precise limits of conductance because they are approached asymptotically and noise in the ionic current is greatly amplified in the extreme segments of the Hill plot. Our approach was predicated on the assumption that the Hill plots achieved a limiting slope within the range of voltage measured. Even if this were true based on a channel's gating mechanism, nonlinearities can arise from the effects of incomplete series resistance and linear capacity compensation, although these were accounted for by simulating an equivalent circuit and the effects were found to be small (Fig. 10).

In conclusion, this study shows that the weak inward rectification in Kir2.1 channels is best explained by an unknown voltage sensor communicating allosterically with the pore gate. The double ramp protocol used in these experiments is a useful tool for uncoupling gating components to reveal both their individual characteristics and the energies of interaction (or coupling con-stants) between them, but conductance Hill analysis depends on being able to accurately measure asymptotic rates of approach at extreme voltages, and so is primarily useful for weak coupling. With these limitations in mind, Hill analysis has the potential for improving our understanding of allosteric coupling in ion channels and proteins in general.

References

Aggarwal, S.K., and R. MacKinnon. 1996. Contribution of the S4 segment to gating charge in the Shaker K+ channel. *Neuron.* 16:1169–1177. https://doi .org/10.1016/S0896-6273(00)80143-9

Banks, H.T., and M.L. Joyner. 2017. AIC under the framework of least squares estimation. *Appl. Math. Lett.* 74:33–45. https://doi.org/10.1016/j.aml.2017 .05.005

Burnham, K.P., and D.R. Anderson. 2004. Multimodel Inference. *Sociol. Methods Res.* 33:261–304. https://doi.org/10.1177/0049124104268644

Chang, H.-K., J.-R. Lee, T.-A. Liu, C.-S. Suen, J. Arreola, and R.-C. Shieh. 2010. The extracellular K+ concentration dependence of outward currents through Kir2.1 channels is regulated by extracellular Na+ and Ca2+. *J. Biol. Chem.* 285:23115–23125. https://doi.org/10.1074/jbc.M110.121186

Cheng, W. 2012. From Bacteria to Human: Biophysical Studies of Inward Rectifying Potassium Channels. PhD dissertation. Washington University in St. Louis. 218 pp.

Chowdhury, S., and B. Chanda. 2010. Deconstructing thermodynamic parameters of a coupled system from site-specific observables. *Proc. Natl. Acad. Sci. USA.* 107:18856–18861. https://doi.org/10.1073/pnas.1003609107

Constanti, A., and M. Galvan. 1983. Fast inward-rectifying current accounts for anomalous rectification in olfactory cortex neurones. *J. Physiol.* 335:153–178. https://doi.org/10.1113/jphysiol.1983.sp014526

Day, M., D.B. Carr, S. Ulrich, E. Ilijic, T. Tkatch, and D.J. Surmeier. 2005. Dendritic excitability of mouse frontal cortex pyramidal neurons is shaped by the interaction among HCN, Kir2, and Kleak channels. *J. Neurosci.* 25:8776–8787. https://doi.org/10.1523/JNEUROSCI.2650-05.2005

Ficker, E., M. Taglialatela, B. Wible, C. Henley, and A. Brown. 1994. Spermine and spermidine as gating molecules for inward rectifier K+ channels. *Science.* 266:1068–1072. https://doi.org/10.1126/science.7973666

González-Pérez, V., K. Stack, K. Boric, and D. Naranjo. 2010. Reduced voltage sensitivity in a K+-channel voltage sensor by electric field remodeling. *Proc. Natl. Acad. Sci. USA.* 107:5178–5183. https://doi.org/10.1073/pnas .1000963107

Guo, D., and Z. Lu. 2000. Pore block versus intrinsic gating in the mechanism of inward rectification in strongly rectifying IRK1 channels. *J. Gen. Physiol.* 116:561–568. https://doi.org/10.1085/jgp.116.4.561

Guo, D., Y. Ramu, A.M. Klem, and Z. Lu. 2003. Mechanism of rectification in inward-rectifier K+ channels. *J. Gen. Physiol.* 121:261–275. https://doi.org/10.1085/jgp.200208771

Hagiwara, S., S. Miyazaki, and N.P. Rosenthal. 1976. Potassium current and the effect of cesium on this current during anomalous rectification of the egg cell membrane of a starfish. *J. Gen. Physiol.* 67:621–638. https://doi.org/10.1085/jgp.67.6.621

Hamill, O.P., A. Marty, E. Neher, B. Sakmann, and F.J. Sigworth. 1981. Improved patch-clamp techniques for high-resolution current recording from cells and cell-free membrane patches. *Pflugers Arch.* 391:85–100. https://doi.org/10.1007/BF00656997

Hibino, H., A. Inanobe, K. Furutani, S. Murakami, I. Findlay, and Y. Kurachi. 2010. Inwardly rectifying potassium channels: their structure, function, and physiological roles. *Physiol. Rev.* 90:291–366. https://doi.org/10.1152/physrev.00021.2009

Hilgemann, D.W. 1995. The giant membrane patch. *In* Single-Channel Recording. Springer US, Boston, MA. pp. 307–327.

Hill, A.V. 1910. The possible effects of the aggregation of the molecules of haemoglobin on its dissociation curves. *J. Physiol.* 40:4–7.

Horn, R. 1987. Statistical methods for model discrimination. Applications to gating kinetics and permeation of the acetylcholine receptor channel. *Biophys. J.* 51:255–263. https://doi.org/10.1016/S0006-3495(87)83331-3

Horrigan, F.T., J. Cui, and R.W. Aldrich. 1999. Allosteric voltage gating of potassium channels I. Mslo ionic currents in the absence of Ca(2+). *J. Gen. Physiol.* 114:277–304. https://doi.org/10.1085/jgp.114.2.277

Hume, J.R., and A. Uehara. 1985. Ionic basis of the different action potential configurations of single guinea-pig atrial and ventricular myocytes. *J. Physiol.* 368:525–544. https://doi.org/10.1113/jphysiol.1985.sp015874

Ishihara, K., and T. Ehara. 2004. Two modes of polyamine block regulating the cardiac inward rectifier K+ current IK1 as revealed by a study of the Kir2.1 channel expressed in a human cell line. *J. Physiol.* 556:61–78. https://doi.org/10.1113/jphysiol.2003.055434

Islas, L.D., and F.J. Sigworth. 1999. Voltage sensitivity and gating charge in Shaker and Shab family potassium channels. *J. Gen. Physiol.* 114:723–742. https://doi.org/10.1085/jgp.114.5.723

Kemmer, G., and S. Keller. 2010. Nonlinear least-squares data fitting in Excel spreadsheets. *Nat. Protoc.* 5:267–281. https://doi.org/10.1038/nprot.2009.182

Kubo, Y., and Y. Murata. 2001. Control of rectification and permeation by two distinct sites after the second transmembrane region in Kir2.1 K+ channel. *J. Physiol.* 531:645–660. https://doi.org/10.1111/j.1469-7793.2001.0645h.x

Kubo, Y., T.J. Baldwin, Y.N. Jan, and L.Y. Jan. 1993. Primary structure and functional expression of a mouse inward rectifier potassium channel. *Nature.* 362:127–133. https://doi.org/10.1038/362127a0

Kurata, H.T., M. Rapedius, M.J. Kleinman, T. Baukrowitz, and C.G. Nichols. 2010. Voltage-dependent gating in a "voltage sensor-less" ion channel. *PLoS Biol.* 8:e1000315. https://doi.org/10.1371/journal.pbio.1000315

Lee, J.-K., S.A. John, and J.N. Weiss. 1999. Novel gating mechanism of polyamine block in the strong inward rectifier K channel Kir2.1. *J. Gen. Physiol.* 113:555–564. https://doi.org/10.1085/jgp.113.4.555

Liu, T.-A., H.-K. Chang, and R.-C. Shieh. 2011. Extracellular K+ elevates outward currents through Kir2.1 channels by increasing single-channel conductance. *Biochim. Biophys. Acta.* 1808:1772–1778. https://doi.org/10.1016/j.bbamem.2011.02.016

Liu, T.-A., H.-K. Chang, and R.-C. Shieh. 2012. Revisiting inward rectification: K ions permeate through Kir2.1 channels during high-affinity block by spermidine. *J. Gen. Physiol.* 139:245–259. https://doi.org/10.1085/jgp.201110736

Lopatin, A.N., E.N. Makhina, and C.G. Nichols. 1994. Potassium channel block by cytoplasmic polyamines as the mechanism of intrinsic rectification. *Nature.* 372:366–369. https://doi.org/10.1038/372366a0

Matsuda, H., A. Saigusa, and H. Irisawa. 1987. Ohmic conductance through the inwardly rectifying K channel and blocking by internal Mg2+. *Nature.* 325:156–159. https://doi.org/10.1038/325156a0

Matsuda, H., K. Oishi, and K. Omori. 2003. Voltage-dependent gating and block by internal spermine of the murine inwardly rectifying K+ channel, Kir2.1. *J. Physiol.* 548:361–371. https://doi.org/10.1113/jphysiol.2003.038844

Matsuda, H., M. Hayashi, and M. Okada. 2010. Voltage-dependent block by internal spermine of the murine inwardly rectifying K+ channel, Kir2.1, with asymmetrical K+ concentrations. *J. Physiol.* 588:4673–4681. https://doi.org/10.1113/jphysiol.2010.194480

Nichols, C.G., and A.N. Lopatin. 1997. Inward rectifier potassium channels. *Annu. Rev. Physiol.* 59:171–191. https://doi.org/10.1146/annurev.physiol.59.1.171

Noble, D. 1979. The initiation of the heartbeat. Clarendon Press, Oxford.

Oishi, K., K. Omori, H. Ohyama, K. Shingu, and H. Matsuda. 1998. Neutralization of aspartate residues in the murine inwardly rectifying K+ channel IRK1 affects the substate behaviour in Mg2+ block. *J. Physiol.* 510:675–683. https://doi.org/10.1111/j.1469-7793.1998.675bj.x

Omori, K., K. Oishi, and H. Matsuda. 1997. Inwardly rectifying potassium channels expressed by gene transfection into the green Monkey kidney cell line COS-1. *J. Physiol.* 499:369–378. https://doi.org/10.1113/jphysiol.1997.sp021934

Schewe, M., E. Nematian-Ardestani, H. Sun, M. Musinszki, S. Cordeiro, G. Bucci, B.L. de Groot, S.J. Tucker, M. Rapedius, and T. Baukrowitz. 2016. A Non-canonical Voltage-Sensing Mechanism Controls Gating in K2P K(+) Channels. *Cell.* 164:937–949. https://doi.org/10.1016/j.cell.2016.02.002

Seoh, S.A., D. Sigg, D.M. Papazian, and F. Bezanilla. 1996. Voltage-sensing residues in the S2 and S4 segments of the Shaker K+ channel. *Neuron.* 16:1159–1167. https://doi.org/10.1016/S0896-6273(00)80142-7

Shieh, R.C., S.A. John, J.K. Lee, and J.N. Weiss. 1996. Inward rectification of the IRK1 channel expressed in Xenopus oocytes: effects of intracellular pH reveal an intrinsic gating mechanism. *J. Physiol.* 494:363–376.

Sigg, D. 2013. A linkage analysis toolkit for studying allosteric networks in ion channels. *J. Gen. Physiol.* 141:29–60. https://doi.org/10.1085/jgp.201210859

Stanfield, P.R., N.W. Davies, P.A. Shelton, M.J. Sutcliffe, I.A. Khan, W.J. Brammar, and E.C. Conley. 1994. A single aspartate residue is involved in both intrinsic gating and blockage by Mg2+ of the inward rectifier, IRK1. *J. Physiol.* 478:1–6. https://doi.org/10.1113/jphysiol.1994.sp020225

Vandenberg, C.A. 1987. Inward rectification of a potassium channel in cardiac ventricular cells depends on internal magnesium ions. *Proc. Natl. Acad. Sci. USA.* 84:2560–2564. https://doi.org/10.1073/pnas.84.8.2560

Yang, J., Y.N. Jan, and L.Y. Jan. 1995. Control of rectification and permeation by residues in two distinct domains in an inward rectifier K+ channel. *Neuron.* 14:1047–1054. https://doi.org/10.1016/0896-6273(95)90343-7

Yifrach, O. 2004. Hill coefficient for estimating the magnitude of cooperativity in gating transitions of voltage-dependent ion channels. *Biophys. J.* 87:822–830. https://doi.org/10.1529/biophysj.104.040410